

# The brightest galaxies at Cosmic Dawn

Charlotte A. Mason<sup>1,2\*</sup>, Michele Trenti<sup>3,4</sup> and Tommaso Treu<sup>5</sup>

<sup>1</sup>*Cosmic Dawn Center (DAWN)*

<sup>2</sup>*Niels Bohr Institute, University of Copenhagen, Jagtvej 128, 2200 København N, Denmark*

<sup>3</sup>*School of Physics, University of Melbourne, Parkville 3010, VIC, Australia*

<sup>4</sup>*ARC Centre of Excellence for All Sky Astrophysics in 3 Dimensions (ASTRO 3D), Australia*

<sup>5</sup>*Department of Physics and Astronomy, University of California, Los Angeles, 430 Portola Plaza, Los Angeles, CA 90095, USA*

Accepted 2023 January 03. Received 2022 December 30; in original form 2022 July 30

## ABSTRACT

Recent JWST observations suggest an excess of  $z \gtrsim 10$  galaxy candidates above most theoretical models. Here, we explore how the interplay between halo formation timescales, star formation efficiency and dust attenuation affects the properties and number densities of galaxies observed in the early universe. To guide intuition, we calculate the theoretical upper limit on the UV luminosity function, assuming star formation is 100% efficient and all gas in halos is converted into stars, and that galaxies are at the peak age for UV emission ( $\sim 10$  Myr). This upper limit is  $\sim 4$  orders of magnitude greater than current observations, implying no formal tension with star formation in  $\Lambda$ CDM cosmology. In a more realistic model, we use the distribution of halo formation timescales derived from extended Press-Schechter theory as a proxy for star formation rate (SFR). We predict that the galaxies observed so far at  $z \gtrsim 10$  are dominated by those with the fastest formation timescales, and thus most extreme SFRs and young ages. These galaxies can be upscattered by  $\sim 1.5$  mag compared to the median UV magnitude vs halo mass relation. This likely introduces a selection effect at high redshift whereby only the youngest ( $\lesssim 10$  Myr), most highly star forming galaxies (specific SFR  $\gtrsim 30 \text{ Gyr}^{-1}$ ) have been detected so far. Furthermore, our modelling suggests that redshift evolution at the bright end of the UV luminosity function is substantially affected by the build-up of dust attenuation. We predict that deeper JWST observations (reaching  $m \sim 30$ ) will reveal more typical galaxies with relatively older ages ( $\sim 100$  Myr) and less extreme specific SFRs ( $\sim 10 \text{ Gyr}^{-1}$  for a  $M_{\text{UV}} \sim -20$  galaxy at  $z \sim 10$ ).

**Key words:** cosmology: theory – cosmology: dark ages, reionisation, first stars – galaxies: high-redshift; – galaxies: evolution

## 1 INTRODUCTION

Discovering when and how the first galaxies formed is still a major unsolved problem in modern astrophysics. Theoretical models predict the formation of the first sources, so-called, ‘Cosmic Dawn’ was underway within the first few hundred million years of the universe’s lifetime,  $z \sim 20\text{--}40$  (e.g., Trenti & Stiavelli 2009; Bromm & Yoshida 2011).

The Hubble Space Telescope has allowed us to observe galaxies out to  $z \sim 10$ , finding some that are relatively bright at rest-frame UV wavelengths (e.g., Zheng et al. 2012; Coe et al. 2013; Oesch et al. 2016; Morishita et al. 2018; Bagley et al. 2022). The rest-frame UV continuum is produced primarily by young ( $\sim 10$  Myr), massive stars, and therefore the UV luminosity function (LF) traces recent star formation. Interpreting these observations requires comparison to theoretical modelling, and the UV LF has been modelled using a range of approaches, from ‘simple’ but efficient semi-empirical models which can identify the main physical drivers of its evolution, (e.g., Trenti et al. 2011; Tacchella et al. 2013; Mason et al. 2015; Sun & Furlanetto 2016; Yung et al. 2019; Mirocha et al. 2020), to semi-analytic models which incorporate more physical processes

and the realistic assembly of dark matter halos from merger trees (e.g., Tacchella et al. 2018; Yung et al. 2019; Hutter et al. 2021), and finally hydrodynamical simulations which aim to model star formation and feedback processes self-consistently (e.g., Ma et al. 2018; Vogelsberger et al. 2020). Most  $z \lesssim 8$  observations of the UV LF can be readily explained under the assumption of no redshift evolution in the star formation efficiency (e.g., Trenti et al. 2011; Mason et al. 2015; Tacchella et al. 2018; Bouwens et al. 2021). However, relative to most theoretical models, an excess of bright galaxies is observed at  $z \gtrsim 8$  (Bowler et al. 2020; Leethochawalit et al. 2022a).

The James Webb Space Telescope (JWST) is pushing our observational horizon even further, expanding our view to  $5\mu\text{m}$  (with the NIRCam instrument, Rieke et al. 2005), making it possible to observe rest-frame UV emission from  $z \lesssim 30$  galaxies, when the universe is just 100 Myr old. Interestingly, recent works have shown JWST to preliminarily confirm HST galaxy counts at  $z \sim 7\text{--}9$  (Leethochawalit et al. 2022b) but claimed discovery of a relatively high number of galaxy candidates at  $z \sim 10\text{--}17$  from early release science observations, suggesting the excess of sources relative to UV LF predictions extends to higher redshifts (Castellano et al. 2022; Naidu et al. 2022; Adams et al. 2022; Morishita & Stiavelli 2022; Donnan et al. 2022; Atek et al. 2022; Finkelstein et al. 2022).

\* E-mail: charlotte.mason@nbi.ku.dk

It is too early to draw definitive conclusions, as these sources are not spectroscopically confirmed and the photometric candidates are based on reductions using preliminary calibrations (indeed, some of the same sources are reported with significantly different fluxes by different groups), and cover small fields subject to cosmic variance (e.g., [Trenti & Stiavelli 2008](#)). Nevertheless, it is exciting to consider what the theoretical upper limit is on the UV LF at high redshift and how to interpret these early observations.

In the standard  $\Lambda$  Cold Dark Matter ( $\Lambda$ CDM) paradigm, galaxies form as gas accretes into dark matter halos (e.g. for recent reviews see, [Somerville & Davé 2015](#); [Wechsler & Tinker 2018](#)). However, the conversion of gas into stars appears to be inefficient, likely due to processes which heat and expel gas, generally described as ‘feedback’ (e.g., [Silk 1997](#)). To investigate the maximum allowed UV LF as a function of redshift, we take a similar approach to [Behroozi & Silk \(2018\)](#) who calculated a theoretical upper limit on stellar masses at  $z > 4$ , in  $\Lambda$ CDM, assuming a 100% star formation efficiency converting gas into stars. Due to order of magnitude uncertainties in measuring stellar mass, depending on assumed star formation histories (e.g., [Whitler et al. 2022](#)), and for easiest comparison to JWST data, we focus here on modelling the UV LF. We will show that by assuming 100% star formation efficiency and very young ages, this upper limit is at least 4 orders of magnitude above current observations and thus such early bright galaxies are not inconsistent with  $\Lambda$ CDM.

Motivated by recent work on the stochasticity of star formation, due to variation in halo formation histories, and its impact on the UV LF shape (e.g., [Ren et al. 2018, 2019](#); [Mirocha et al. 2021](#); [Furlanetto & Mirocha 2022](#)), we assess whether UV bright galaxies can arise naturally as outliers from the general population, thanks to their very young ages and high star formation rates. We will show that current samples at  $z \gtrsim 10$ , as a result of selection at relatively bright fluxes ( $m_{\text{AB}} < 29$ ,  $M_{\text{UV}} \lesssim -19$ ), are dominated by extremely young, rapidly star-forming galaxies.

This paper is structured as follows: we describe our method for calculating the UV LF in Section 2, we present our results in Section 3 and conclude in Section 4. We assume a flat  $\Lambda$ CDM cosmology with  $\Omega_m = 0.3$ ,  $\Omega_\Lambda = 0.7$ ,  $h = 0.7$  and magnitudes are in the AB system.

## 2 METHODS

UV continuum emission from galaxies is dominated by light from young stars ( $\sim 10$  Myr), thus the UV emission traces the recent star formation history of a galaxy (e.g., [Stark et al. 2009](#)). High UV luminosities are produced by galaxies with very high star formation rates and young ages. The increasing presence of high equivalent width (EW) nebular emission lines with redshift implies galaxies in the early universe are very young and rapidly forming stars (e.g., [Labbé et al. 2013](#); [Stark et al. 2013](#); [Smit et al. 2014](#); [Reddy et al. 2018](#); [Boyet et al. 2022](#); [Stefanon et al. 2022](#)).

We model the UV LF following the prescription by [Mason et al. \(2015, hereafter M15\)](#), which provides an accurate description of observations at  $z \lesssim 8$ . We assume that gas accretes at the same rate as dark matter and use extended Press-Schechter theory to calculate the evolution of dark matter halo properties ([Bond et al. 1991](#)), as is commonly done by many other semi-empirical and semi-analytic models of the luminosity function (e.g., [Trenti et al. 2011](#); [Tacchella et al. 2013](#); [Behroozi & Silk 2015](#); [Sun & Furlanetto 2016](#); [Yung et al. 2019](#)).

A more realistic treatment of accretion rates can be obtained from merger trees in N-body simulations (e.g., [Liu et al. 2016](#); [Tacchella](#)

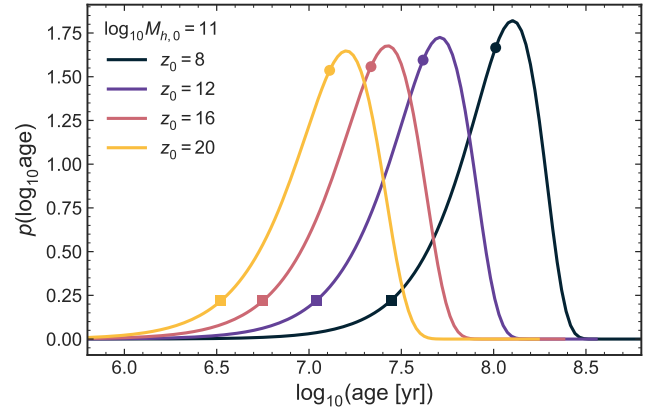


**Figure 1.** Probability distribution of ‘ages’ – the time in which a halo with mass  $M_{h,0}$  at  $z_0$  assembled half its mass. The coloured lines show a range of observed redshifts for a halo of mass  $10^{11} M_{\odot}$ . The circles show the position of the median formation time, the squares shows the lowest 10% of ages.

et al. 2018; [Hutter et al. 2021](#); [Mirocha et al. 2021](#)) or hydrodynamical simulations (e.g., [Vogelsberger et al. 2020](#); [Wilkins et al. 2022](#)) in order to model the high redshift UV LF. However, these simulations are volume-limited and  $< 1$  Gpc simulations do not provide sufficient statistics to understand how the rarest, brightest, sources form. For example, [Mutch et al. \(2016\)](#) identified only two galaxies as bright as GNz11 in the MERAXES semi-analytic model (though, with increasing computing power, larger N-body simulations are becoming feasible for exploring rare high-redshift sources, e.g., [Oogi et al. 2022](#)). In this work we use the distribution of halo formation times from extended Press-Schechter theory, assuming ellipsoidal collapse, to calculate timescales for star formation. Using this analytic approach we can build our model over an, in principle, unlimited range of halo masses.

To model the accretion rate of halos, we consider the ‘halo formation timescale’ – the time in which a halo doubles in mass. The distribution of halo formation times (e.g., [Giocoli et al. 2007](#)) is:

$$p(w)dw = 2w \operatorname{erfc}\left(\frac{w}{\sqrt{2}}\right). \quad (1)$$

Here,  $w$  is a time variable:

$$w(M_h) = \sqrt{q} \frac{\delta_c(z_f) - \delta_c z_0}{\sqrt{\sigma^2(M_h/2) - \sigma^2(M_h)}} \quad (2)$$

where  $\delta_c(z) \equiv \delta_c(0)/D(z)$  is the overdensity required for spherical collapse at  $z$ , where  $\delta_c(0) \approx 1.686$  and  $D(z)$  is the linear growth factor, and  $\sigma^2(M)$  is the variance of the linear fluctuation field, smoothed with a top-hat filter with scale  $R = (3M_h/4\pi\bar{\rho})^{1/3}$  where  $\bar{\rho}$  is the comoving density.

Figure 1 shows the predicted formation time (which we will refer to as ‘age’) distribution for a  $10^{11} M_{\odot}$  halo observed at  $z \geq 8$ . Here we have converted from  $p(w)dw$  to  $p(\log_{10} t)d \log_{10} t$  numerically. A broad distribution of formation times is predicted for a given halo mass, with 10% of halos having assembled  $\sim 5\times$  faster than the median of the distribution. As the majority of UV emission comes from  $\sim 10$  Myr old stars, and SFRs are likely to track the halo formation timescale (assuming gas follows dark matter), the low age tail of this distribution is likely to be extremely UV bright. We note the similarity of this distribution to the age distribution derived from SED fitting of high redshift galaxies (e.g., [Whitler et al.](#)

2022), implying our assumption of star formation tracing halo mass accretion is reasonable.

We model galaxies' star formation histories (SFR) as increasing step functions as the halos accrete gas on the timescales defined above. This approximates rapidly rising SFRs seen in simulations at high redshift (e.g., [Finlator et al. 2011](#); [Ceverino et al. 2018](#); [Mirocha et al. 2021](#); [Legrand et al. 2022](#)). We thus define the SFR as a function of the halo formation timescale. The SFR of a halo with mass  $M_h$  (at lookback time  $t_0$ ), which had mass  $M_h/2^i$  at lookback time  $t_i$ , between timestep  $t_i$  and  $t_{i+1}$  is:

$$\text{SFR}(M_h, t_i, t_{i+1}) = f_b \frac{M_h \epsilon_{\text{SF}}(M_h/2^i)}{2^i (t_{i+1} - t_i)} \quad (3)$$

where  $f_b \equiv \Omega_b/\Omega_m = 0.162$  is the cosmic baryon fraction and  $\epsilon_{\text{SF}}(M_h)$  is the star formation efficiency. The time interval  $t_{i+1} - t_i$  is the halo formation (doubling) time, as a function of mass and redshift, as defined in Equations 1 and 2, and the factor  $2^i$  accounts for the doubling of halo mass in each step. We refer the reader to Figure 2 by [Mason et al. \(2015\)](#) for a clear visualisation of these SFH models.

As in the [M15](#) model we assume  $\epsilon_{\text{SF}}$  is a function of halo mass but not of redshift (consistent with other semi-analytic modelling efforts and with inferences from observations, see e.g., [Trenti et al. 2011](#); [Tacchella et al. 2018](#); [Bouwens et al. 2021](#); [Harikane et al. 2022](#)). Due to the very young age of the universe at  $z \gtrsim 10$  and the rapid halo formation timescales that we will discuss below, this prescription for star formation histories leads to increasingly high SFR rates at early time, leading to SFH which are rapidly rising, mimicking the effects of recent and on-going star formation bursts.

To compute the UV luminosity of each galaxy we populate halos with stellar populations using the simple stellar population (SSP) models of [Bruzual & Charlot \(2003\)](#). We assume a Salpeter initial mass function between  $0.1 - 100 M_\odot$  and a constant stellar metallicity of  $Z = 0.01 Z_\odot$ . We neglect redshift evolution in metallicity under the assumption that very early star formation has already enriched the gas (e.g., [Trenti & Stiavelli 2009](#)), and note that metallicities do not significantly affect the non-ionizing UV continuum luminosity (e.g., [Schaerer 2003](#)). The UV luminosity of a galaxy is given by:

$$L_{\text{UV}}(M_h) = \sum_{i=0}^N \text{SFR}(M_h, t_i, t_{i+1}) \int_{t_i}^{t_{i+1}} dt \mathcal{L}_{\text{SSP}}(t) \quad (4)$$

where  $\mathcal{L}_{\text{SSP}}(t)$  is the luminosity at  $1500 \text{\AA}$  of a SSP of mass  $1 M_\odot$  and age  $t$ . We consider two star formation steps, which [M15](#) demonstrated were sufficient to model the majority of the UV luminosity.

The stellar mass formed in a dark matter halo with mass  $M_h$ :

$$M_\star(M_h) = f_b M_h \sum_{i=0}^N \frac{\epsilon_{\text{SF}}(M_h/2^i)}{2^i} \quad (5)$$

Most semi-empirical models of the UV LF considered only a single star formation timescale (e.g., [Trenti et al. 2010](#); [Mason et al. 2015](#); [Park et al. 2019](#)). Here, we will sample timescales from Equation 1 to calculate SFRs (Equation 3). As discussed by [Ren et al. \(2019\)](#) and [Mirocha et al. \(2021\)](#), adding scatter to the relation between UV luminosity and halo mass requires recalibrating  $\epsilon_{\text{SF}}$  to ensure models match the observed UV LFs. In this work we neglect this recalibration, as the effect only becomes significant for halos with masses  $> 10^{11} M_\odot$ , for which we expect very few at  $z > 10$ . We thus use the  $\epsilon_{\text{SF}}(M_h)$  calibrated by [M15](#) at  $z \sim 5$  and do not expect this to have a strong impact on our results.

The UV luminosity function is then:

$$\Phi(M_{\text{UV}}) = \phi(M_h) \left| \frac{dM_h}{dM_{\text{UV}}} \right| \quad (6)$$

where  $dM_h/dM_{\text{UV}} = \ln 10 M_h / 2.5$  and we can invert the  $L(M_h)$  relation in Equation 4 above to find  $M_{\text{UV}}(M_h)$ . In the following we assume the [Reed et al. \(2007\)](#) halo mass function (HMF) which was simulated specifically for  $z \sim 10 - 30$  halos, and is consistent with other HMFs (e.g., [Sheth et al. 2001](#)) at lower redshifts. We use the python package `hmf` ([Murray et al. 2013](#)) to calculate the halo mass function and use the [Eisenstein & Hu \(1998\)](#) matter transfer function.

## 3 RESULTS

### 3.1 An upper limit on the UV LF

To derive an upper limit on the UV LF we follow [Behroozi & Silk \(2018\)](#) and consider the case of maximally efficient star formation, where all the gas is converted into stars  $M_\star = f_b M_h$ , i.e. the star formation efficiency is  $\epsilon_{\text{SF}} = 1$ , and ages for galaxies where they are at their peak emission of UV photons.

We calculate the maximum UV LFs at  $z \sim 8 - 20$  using Equations 4 and 6 above, assuming 100% star formation efficiency and one period of constant star formation,  $\text{SFR} = f_b M_h \epsilon_{\text{SF}} / t_{\text{age}}$ , over  $t_{\text{age}} = 10^7$  Myr. We assume  $t_{\text{age}} = 10^7$  Myr as the majority of UV continuum photons are emitted during this period (e.g., [Schaerer 2003](#)). This results in a specific star formation rate (sSFR)  $100 \text{ Gyr}^{-1}$ , which is consistent with the highest sSFR at  $z \gtrsim 6$  ([Stark et al. 2013](#); [Santini et al. 2017](#); [Endsley et al. 2021](#)).

Our resulting LF is plotted in Figure 2. We also plot the UV LF modelled as described in Section 2, using a mass-dependent, but redshift-independent efficiency,  $\epsilon_{\text{SF}}(M_h)$ , as derived by [M15](#), with and without dust attenuation. The maximum theoretical LF is at least four orders of magnitude higher than the observations and the [M15](#) model, and the ratio between the maximum limit and the mass-dependent efficiency model increases with increasing redshift. This is because, in the [M15](#) model, galaxies have younger ages (because of higher accretion rates) and lower halo masses (because lower mass galaxies can be young and bright) at fixed  $M_{\text{UV}}$  and redshift. While the star formation efficiency does not evolve with halo mass in the model, the star formation efficiency as a function of  $M_{\text{UV}}$  is thus lower at fixed  $M_{\text{UV}}$  with increasing redshift.

We can also see dust attenuation is the dominant factor in the Schechter function shape of our model LF. In the [M15](#) model we use the [Meurer et al. \(1999\)](#) attenuation law  $A_{\text{UV}} = 4.43 + 1.99\beta$ , modelling UV slope  $\beta(M_{\text{UV}}, z)$  empirically from observations by [Bouwens et al. \(2014\)](#). Past the limits of these observations we assume  $\beta(M_{\text{UV}}, z > 8) = \beta(M_{\text{UV}}, z = 8)$ . However, in the early universe, it is plausible that limited dust has been produced in the majority of young galaxies. Simulations of very low metallicity  $Z \sim 0.01 Z_\odot$  galaxies predict limited dust formation by core collapse supernovae and UV slopes  $\beta \sim -2.5$  ([Jaacks et al. 2018](#)). Early JWST observations have also found evidence for such blue UV slopes at  $4 < z < 7$  ([Nanayakkara et al. 2022](#)). For  $\beta \sim -2.5$  the attenuation is negligible, resulting in the dashed lines in Figure 2, where the model follows the power-law shape of the HMF more closely. Thus a reduction in dust attenuation may play an important role in explaining excesses of bright  $z \gtrsim 8$  galaxies (e.g., [Bowler et al. 2020](#)). Indeed, we note that of the brightest  $z \gtrsim 11$  candidates found with JWST, all show very blue UV slopes  $\beta \lesssim -2.1$ , indicating negligible dust attenuation ([Naidu et al. 2022](#); [Atek et al. 2022](#); [Donnan et al. 2022](#)). Though c.f. recent ALMA detections of dust continuum in 'normal'  $z \sim 7$  galaxies

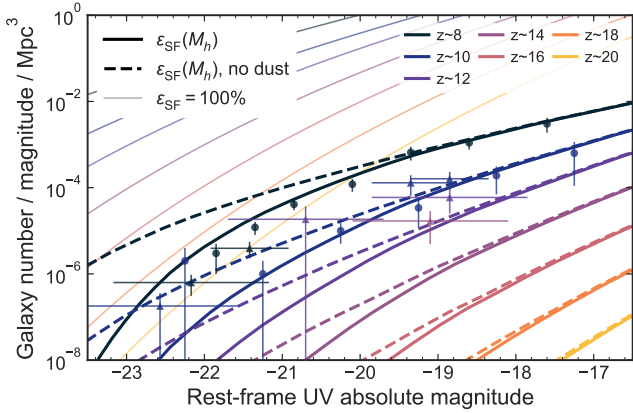


**Figure 2.** UV luminosity function assuming 100% star formation efficiency (thick solid lines) from  $z \sim 8$ –20. For illustration, we also show a model which assumes a lower, halo mass-dependent, star formation efficiency (extending the M15, model to  $z > 16$ ). Solid lines show the model including dust attenuation, dashed lines show the model without dust attenuation. Also shown (datapoints with errorbars) are recent constraints on the UV from HST, UltraVista and JWST at  $z \sim 8$ –10 by Bouwens et al. (2021, circles) and  $z \sim 8$ –14 by Donnan et al. (2022, triangles).

(e.g., Watson et al. 2015; Inami et al. 2022; Schouws et al. 2022). Clearly, an improved understanding of dust attenuation is crucial for interpreting high redshift galaxy observations.

### 3.2 The brightest galaxies are the youngest

While the above upper limit is a useful illustrative constraint, 100% star formation efficiency is very unlikely. Observational constraints on the stellar-to-halo mass relation and most theoretical models require  $\epsilon_{SF} \times f_b \sim 1\%$  (e.g., Behroozi et al. 2013; Sun & Furlanetto 2016). However, as described above, very young galaxies ( $\sim 10$  Myr) will have maximally high UV continuum emission.

We now consider the hypothesis that the majority of galaxies observed at  $z \gtrsim 10$  are outliers in the populations, with very rapid star formation rates and young ages. This hypothesis has already been suggested as an explanation for the highest redshift spectroscopically confirmed galaxy, GNz11 (Oesch et al. 2016; Mutch et al. 2016). To test this hypothesis we now use the distribution of halo formation times (Equation 1) to calculate SFRs.

Figure 3 shows halo mass versus UV magnitude at a range of redshifts. Here we sample 1000 halos with mass  $M_h > 10^7 M_\odot$  and draw halo formation timescales for each halo in order to calculate SFRs and UV luminosity as described in Section 2. We compare these sampled galaxies to the  $M_{UV} - M_h$  relation obtained using the median halo mass distribution. We note that we expect UV luminosities to increase at fixed mass with increasing redshift, as halos assemble faster at higher redshift (see Figure 1).

We see the majority of galaxies that are observable within current limits are outliers in the  $M_{UV} - M_h$  relation, as previously shown by Ren et al. (2019). Here we have demonstrated that it is young ages which significant upscatter galaxies to UV magnitudes up to 1.5 mag above the median relation. Thus, current studies with JWST can probably only detect the youngest, highly star forming tip of the iceberg of the galaxy population (Santini et al. 2022). With deeper data throughout Cycle 1 and beyond, we may expect to reach  $m_{AB} \sim$

30. At these depths we predict it will be possible to observe older, more typical galaxies with ages  $\sim 100$  Myr at  $z \sim 10$ –14.

Finally, we make a forecast for the magnitude distribution of galaxies at  $z > 10$ . In order to have enough statistics we forecast an area of 1 sq. degrees. Based on this area we draw halos from the halo mass function in comoving volume bins corresponding to  $\Delta z = 1$ . For computational efficiency if the number of expected halos is greater than 1000, we set the sampled number to 1000. We then sample halo formation times for each halos using Equation 1 and then calculate the observed UV luminosity of each galaxy, adding dust attenuation as described in Section 3.1. Figure 4 shows the distribution of apparent magnitudes (in the NIRCcam band covering rest-frame 1500 Å) for galaxies in this area as a function of observed redshift and halo formation timescale. We assigned redshifts in each bin by drawing from a uniform distribution  $U \sim [z_0 - 0.5, z_0 + 0.5]$ .

This figure again demonstrates that with increasing redshift, we predict observable galaxies to be increasingly young, with ages  $\lesssim 10$  Myr. At  $z \sim 10$  our model predicts  $M_{UV} \sim -20$  galaxies will have  $sSFR \gtrsim 30 \text{ Gyr}^{-1}$  (as seen in the brightest population already at  $z \sim 7$ , Endsley et al. 2021). As described above, at fixed mass or  $M_{UV}$  we expect galaxies to have increasingly young ages at higher redshifts due to more rapid accretion. However, there is also a selection effect in a magnitude-limited survey: at fixed mass we will only be able to see the youngest galaxies, the median galaxy will be older and fainter. Therefore, current JWST studies are likely to be observing the most extreme sites of star formation in the early universe. We predict that future surveys reaching  $m_{AB} \sim 30$  will instead identify a higher proportion of ‘older’ galaxies ( $\sim 100$  Myr) at  $z \sim 8$ –12, where we predict  $M_{UV} \sim -19$  galaxies will have  $sSFR \sim 10 \text{ Gyr}^{-1}$ .

We note that if dust attenuation decreases at  $z > 10$ , all of our results can be shifted up by  $\sim 1$  mag.

## 4 CONCLUSIONS

We have explored how the interplay between star formation efficiency, galaxy ages and dust attenuation affects the observability of  $z \gtrsim 10$  galaxies. Our conclusions are as follows:

(i) To guide intuition, we derive a theoretical upper limit on the UV LF assuming maximally efficient star formation and young ages which maximise UV emission (10 Myr). Recent  $z > 8$  observations, including candidates discovered in JWST/NIRCcam data, which show an excess of bright galaxies above theoretical models for the UV LF, are fully consistent with this theoretical upper limit on the LF, which is at least four orders of magnitude higher than the data. Therefore, there is no formal tension between current JWST observations at  $z > 10$  and formation of galaxies inside  $\Lambda$ CDM dark-matter halos.

(ii) We find dust attenuation drives the Schechter function shape of our UV LF model at  $z \gtrsim 10$ . If dust attenuation is negligible in galaxies’ first few 100 Myr, this could explain recent observations indicating a power-law LF at  $z \gtrsim 8$ . A better understanding of dust attenuation at  $z > 8$  is thus crucial for interpreting high redshift observations.

(iii) Using the distribution of halo formation times we find the majority of currently detectable galaxies ( $m_{AB} < 29$ ) lie significantly above the median  $M_{UV} - M_h$  relation, and are so bright because they are young and rapidly assembling. This suggests galaxies currently observed at  $z \gtrsim 10$  are likely to be the most extreme tip of the iceberg in terms of star formation, but are unlikely to be representative of the overall galaxy population.

(iv) We predict that within Cycle 1 of JWST, deeper surveys that

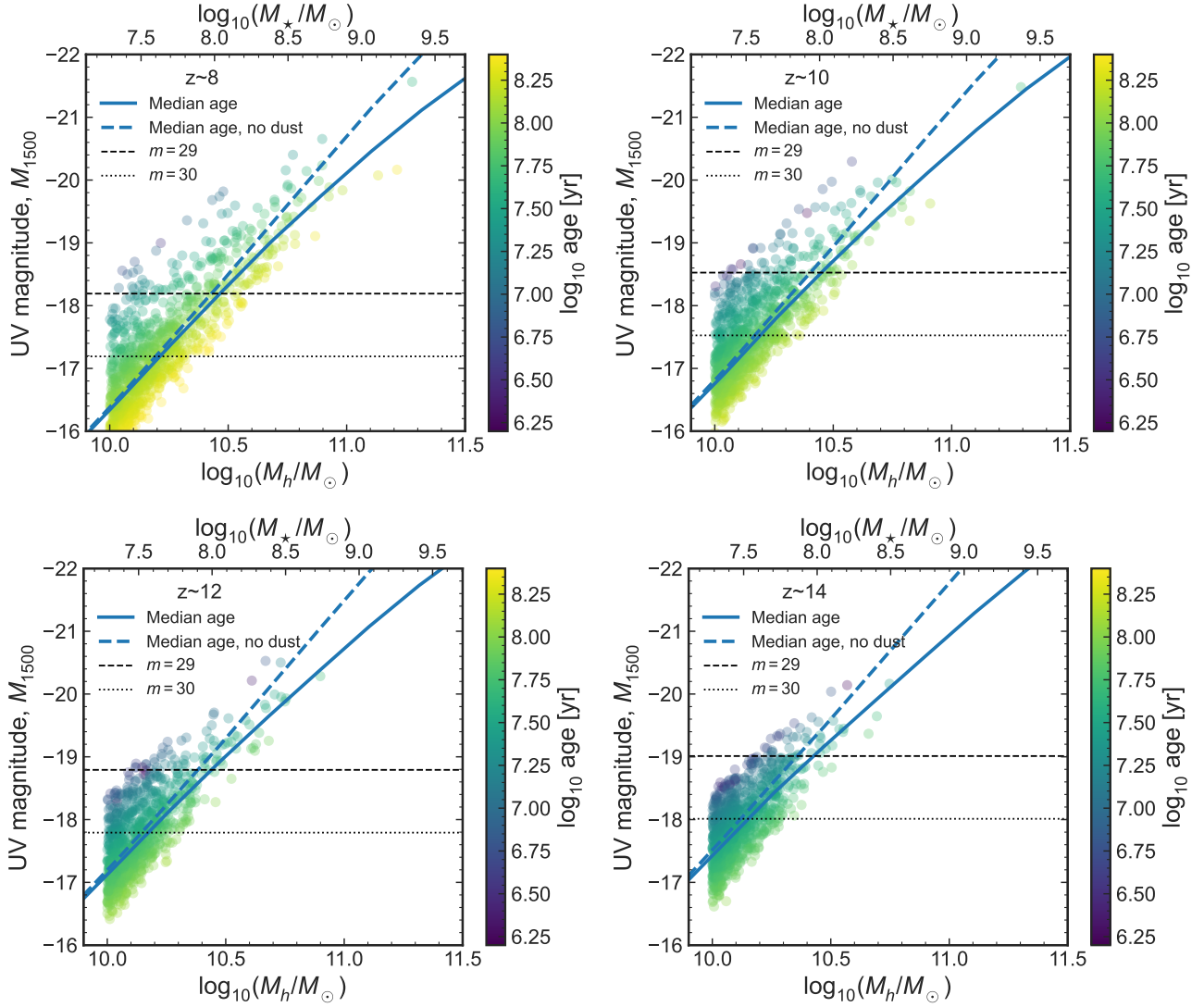


**Figure 3.** UV magnitude, including dust attenuation, as a function of halo mass at  $z \sim 8 - 14$ . Points show 1000 sampled halos at each redshift, coloured by their formation time (time to form half their halo mass). We also show the relation obtained using the median formation timescale (solid blue line, including dust attenuation, dashed blue line, no dust attenuation). The dashed (dotted) horizontal line marks UV magnitude corresponding to  $m_{\text{AB}} = 29(30)$ , typical limits for current and upcoming NIRC*am* imaging (e.g., [Merlin et al. 2022](#)). The majority of detectable galaxies lie significantly above the relation obtained using the median formation timescale – young galaxies are upscattered to bright UV magnitudes.

will reach  $m_{\text{AB}} < 30$  will detect older ( $\sim 100$  Myr) galaxies, more typical of the population at fixed mass.

We predict early JWST observations of  $z \gtrsim 10$  galaxies will be dominated by young galaxies with very high star formation rates, which are scattered up to 1.5 mag above the median  $M_{\text{UV}} - M_h$  relation. While ages are challenging to measure at high redshift from SEDs (e.g., [Laporte et al. 2021](#); [Tacchella et al. 2022](#); [Whitler et al. 2022](#)), this is consistent with the increasing presence of strong nebular line emission in the brightest galaxy samples at  $z \gtrsim 7$  (e.g., [Endsley et al. 2021](#)), indicating very recent star formation and high sSFR. It is also interesting to compare with early JWST results which find similar rest-frame UV and optical morphologies and sizes at  $z \gtrsim 7$  ([Chen et al. 2022](#); [Treu et al. 2022](#); [Yang et al. 2022](#)), consistent with the hypothesis these galaxies will have only recently formed the bulk of their stars with very high sSFR.

JWST observations will enable us to understand the most extreme

star-forming systems in the early universe. We predict the bias towards observing very young ages and high specific star formation rates means we will detect increasingly compact, clumpy galaxies (e.g., [Vanzella et al. 2022](#)) with very high EW line emission. We expect more typical early galaxies, with more mature ages ( $\sim 100$  Myr), will become visible at  $z \sim 10 - 14$  in surveys that can reach  $m_{\text{AB}} < 30$ , bringing us closer to completing the picture of galaxy build up at Cosmic Dawn.

#### ACKNOWLEDGEMENTS

We thank Dan Stark for useful discussions. CAM acknowledges support by the VILLUM FONDEN under grant 37459. The Cosmic Dawn Center (DAWN) is funded by the Danish National Research Foundation under grant DNRF140. MT acknowledges support by the Australian Research Council Centre of Excellence for All Sky

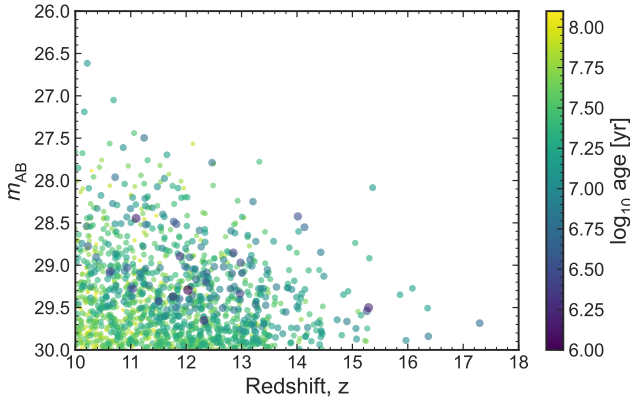


**Figure 4.** Predicted galaxy apparent magnitudes (in the NIRCcam band covering rest-frame 1500Å) as a function of redshift, coloured by halo formation timescale, in a 1 sq degree survey. We add dust attenuation assuming the same  $\beta(M_{UV})$  relation as at  $z \sim 8$ , if dust attenuation is negligible at high redshift galaxies in  $> 10^{10.5} M_{\odot}$  halos may be 1 – 2 mag brighter (see Figure 3).

Astrophysics in 3 Dimensions (ASTRO 3D), through project number CE170100013. TT acknowledges support from NASA through grant JWST-ERS-1324.

#### DATA AVAILABILITY

Tabulated version of the UV LF predictions are available online at: [https://github.com/charlottenosam/UVLF\\_model](https://github.com/charlottenosam/UVLF_model)

#### REFERENCES

Adams N. J., et al., 2022, arXiv e-prints, p. [arXiv:2207.11217](https://arxiv.org/abs/2207.11217)  
Atek H., et al., 2022, *MNRAS*,  
Bagley M. B., et al., 2022, p. [arXiv:2205.12980](https://arxiv.org/abs/2205.12980)  
Behroozi P. S., Silk J., 2015, *ApJ*, 799, 32  
Behroozi P., Silk J., 2018, *MNRAS*, 477, 5382  
Behroozi P. S., Marchesini D., Wechsler R. H., Muzzin A., Papovich C., Stefanon M., 2013, *ApJ*, 777, L10  
Bond J. R., Cole S., Efstathiou G., Kaiser N., 1991, *ApJ*, 379, 440  
Bouwens R. J., et al., 2014, *ApJ*, 793, 115  
Bouwens R. J., et al., 2021, *AJ*, 162, 47  
Bowler R. A. A., Jarvis M. J., Dunlop J. S., McLure R. J., McLeod D. J., Adams N. J., Milvang-Jensen B., McCracken H. J., 2020, *MNRAS*, 493, 2059  
Boyett K. N. K., Stark D. P., Bunker A. J., Tang M., Maseda M. V., 2022, *MNRAS*, 513, 4451  
Bromm V., Yoshida N., 2011, *ARA&A*, 49, 373  
Bruzual G., Charlot S., 2003, *MNRAS*, 344, 1000  
Castellano M., et al., 2022, *ApJ*, 938, L15  
Ceverino D., Klessen R. S., Glover S. C. O., 2018, *MNRAS*, 480, 4842  
Chen Z., Stark D. P., Endsley R., Topping M., Whittler L., Charlot S., 2022, p. [arXiv:2207.12657](https://arxiv.org/abs/2207.12657)  
Coe D., et al., 2013, *ApJ*, 762, 32  
Donnan C. T., et al., 2022, p. [arXiv:2207.12356](https://arxiv.org/abs/2207.12356)  
Eisenstein D. J., Hu W., 1998, *ApJ*, 496, 605  
Endsley R., Stark D. P., Chevallard J., Charlot S., 2021, *MNRAS*, 500, 5229  
Finkelstein S. L., et al., 2022, p. [arXiv:2207.12474](https://arxiv.org/abs/2207.12474)  
Finlator K., Oppenheimer B. D., Davé R., 2011, *MNRAS*, 410, 1703  
Furlanetto S. R., Mirocha J., 2022, *MNRAS*, 511, 3895  
Giocoli C., Moreno J., Sheth R. K., Tormen G., 2007, *MNRAS*, 376, 977  
Harikane Y., et al., 2022, *ApJS*, 259, 20

Hutter A., Dayal P., Yepes G., Gottlöber S., Legrand L., Ucci G., 2021, *MNRAS*, 503, 3698  
Inami H., et al., 2022, *MNRAS*,  
Jaacks J., Finkelstein S. L., Bromm V., 2018, *MNRAS*, 475, 3883  
Labbé I., et al., 2013, *ApJ*, 777, L19  
Laporte N., Meyer R. A., Ellis R. S., Robertson B. E., Chisholm J., Roberts-Borsani G. W., 2021, *MNRAS*, 505, 3336  
Leethochawalit N., Roberts-Borsani G., Morishita T., Trenti M., Treu T., 2022a, p. [arXiv:2205.15388](https://arxiv.org/abs/2205.15388)  
Leethochawalit N., et al., 2022b, p. [arXiv:2207.11135](https://arxiv.org/abs/2207.11135)  
Legrand L., Hutter A., Dayal P., Ucci G., Gottlöber S., Yepes G., 2022, *MNRAS*, 509, 595  
Liu C., Mutch S. J., Angel P. W., Duffy A. R., Geil P. M., Poole G. B., Mesinger A., Wyithe J. S. B., 2016, *MNRAS*, 462, 235  
Ma X., et al., 2018, *MNRAS*, 478, 1694  
Mason C. A., Trenti M., Treu T., 2015, *ApJ*, 813, 21  
Merlin E., et al., 2022, *ApJ*, 938, L14  
Meurer G. R., Heckman T. M., Calzetti D., 1999, *ApJ*, 521, 64  
Mirocha J., Mason C., Stark D. P., 2020, [arXiv:2005.07208](https://arxiv.org/abs/2005.07208) [astro-ph]  
Mirocha J., La Plante P., Liu A., 2021, *MNRAS*, 507, 3872  
Morishita T., Stiavelli M., 2022, p. [arXiv:2207.11671](https://arxiv.org/abs/2207.11671)  
Morishita T., et al., 2018, *ApJ*, 867, 150  
Murray S. G., Power C., Robotham A. S. G., 2013, *Astronomy and Computing*, 3, 23  
Mutch S. J., Geil P. M., Poole G. B., Angel P. W., Duffy A. R., Mesinger A., Wyithe J. S. B., 2016, *MNRAS*, 462, 250  
Naidu R. P., et al., 2022, *ApJ*, 940, L14  
Nanayakkara T., et al., 2022, p. [arXiv:2207.13860](https://arxiv.org/abs/2207.13860)  
Oesch P. A., et al., 2016, *ApJ*, 819, 129  
Oogi T., et al., 2022, arXiv e-prints, p. [arXiv:2207.14689](https://arxiv.org/abs/2207.14689)  
Park J., Mesinger A., Greig B., Gillet N., 2019, *MNRAS*, 484, 933  
Reddy N. A., et al., 2018, *ApJ*, 869, 92  
Reed D. S., Bower R., Frenk C. S., Jenkins A., Theuns T., 2007, *MNRAS*, 374, 2  
Ren K., Trenti M., Mutch S. J., 2018, *ApJ*, 856, 81  
Ren K., Trenti M., Mason C. A., 2019, *ApJ*, 878, 114  
Rieke M. J., Kelly D., Horner S., 2005, in Heaney J. B., Burriesci L. G., eds, Society of Photo-Optical Instrumentation Engineers (SPIE) Conference Series Vol. 5904, Cryogenic Optical Systems and Instruments XI. pp 1–8, doi:10.1117/12.615554  
Santini P., et al., 2017, *ApJ*, 847, 76  
Santini P., et al., 2022, p. [arXiv:2207.11379](https://arxiv.org/abs/2207.11379)  
Schaerer D., 2003, *A&A*, 397, 527  
Schouws S., et al., 2022, *ApJ*, 928, 31  
Sheth R. K., Mo H. J., Tormen G., 2001, *MNRAS*, 323, 1  
Silk J., 1997, *ApJ*, 481, 703  
Smit R., et al., 2014, *ApJ*, 784, 58  
Somerville R. S., Davé R., 2015, *ARA&A*, 53, 51  
Stark D. P., Ellis R. S., Bunker A., Bundy K., Targett T., Benson A., Lacy M., 2009, *ApJ*, 697, 1493  
Stark D. P., Schenker M. A., Ellis R., Robertson B., McLure R., Dunlop J., 2013, *ApJ*, 763, 129  
Stefanon M., Bouwens R. J., Labbé I., Illingworth G. D., Oesch P. A., van Dokkum P., Gonzalez V., 2022, *ApJ*, 927, 48  
Sun G., Furlanetto S. R., 2016, *MNRAS*, 460, 417  
Tacchella S., Trenti M., Carollo C. M., 2013, *ApJ*, 37, L37  
Tacchella S., Bose S., Conroy C., Eisenstein D. J., Johnson B. D., 2018, *ApJ*, 868, 92  
Tacchella S., et al., 2022, *ApJ*, 927, 170  
Trenti M., Stiavelli M., 2008, *ApJ*, 676, 767  
Trenti M., Stiavelli M., 2009, *ApJ*, 694, 879  
Trenti M., Stiavelli M., Bouwens R. J., Oesch P., Shull J. M., Illingworth G. D., Bradley L. D., Carollo C. M., 2010, *ApJ*, 714, L202  
Trenti M., et al., 2011, *ApJ*, 727, L39  
Treu T., et al., 2022, p. [arXiv:2207.13527](https://arxiv.org/abs/2207.13527)  
Vanzella E., et al., 2022, *A&A*, 659, A2  
Vogelsberger M., et al., 2020, *MNRAS*, 492, 5167

- Watson D., Christensen L., Knudsen K. K., Richard J., Gallazzi A., Michałowski M. J., 2015, *Nature*, 519, 327
- Wechsler R. H., Tinker J. L., 2018, *ARA&A*, 56, 435
- Whitler L., Stark D. P., Endsley R., Leja J., Charlot S., Chevallard J., 2022, p. [arXiv:2206.05315](https://arxiv.org/abs/2206.05315)
- Wilkins S. M., et al., 2022, arXiv e-prints, p. [arXiv:2204.09431](https://arxiv.org/abs/2204.09431)
- Yang L., et al., 2022, arXiv e-prints, p. [arXiv:2207.13101](https://arxiv.org/abs/2207.13101)
- Yung L. Y. A., Somerville R. S., Popping G., Finkelstein S. L., Ferguson H. C., Davé R., 2019, *MNRAS*, 490, 2855
- Zheng W., et al., 2012, *Nature*, 489, 406

This paper has been typeset from a  $\text{\TeX/L\AA\TeX}$  file prepared by the author.